Chiral Bloch states in single-layer graphene with Rashba spin-orbit coupling: Equilibrium spin current

Y. Avishai[1] and Y. B. Band[2]

[1]*Department of Physics, Ben-Gurion University of the Negev, Beer-Sheva 8410501, Israel; New York University and the NYU-ECNU Institute of Physics at NYU Shanghai, 3663 Zhongshan Road North, Shanghai 200062, China; and Yukawa Institute for Theoretical Physics, Kyoto 606-8502, Japan*

[2]*Department of Physics, Department of Chemistry, Department of Electro-Optics, and The Ilse Katz Center for Nano-Science, Ben-Gurion University of the Negev, Beer-Sheva 8410501, Israel*

(Received 12 March 2021; accepted 21 July 2021; published 9 August 2021)

Focusing on *equilibrium spin current density tensor*, we analyze the spin physics of electrons in single layer graphene subject to a one-dimensional periodic Kronig-Penney potential $u(x)$ and *uniform* Rashba spin-orbit coupling of strength λ. The combination of Dirac theory of massless two-dimensional electrons, Klein paradox, spin-orbit coupling, and the Bloch theorem yields peculiar features relevant to graphene spintronics. For transverse wave number $k_y = 0$, we show that: (1) The charge current and the spin density vector vanish. (2) Yet, the components J_{xy}, J_{yx}, J_{zy} of the equilibrium spin current density tensor are finite, oscillating in space, with amplitudes that increase quadratically for small λ and then linearly with λ. Quite remarkably, $J_{zy}(x) \neq 0$, that is, the spin is polarized along z, perpendicular to the graphene plane. (3) Due to the continuity equation, the space dependence of the spin current density $J_{yx}(x)$ is associated with a finite spin torque density $\mathcal{T}_y(x) = \frac{\partial J_{yx}(x)}{\partial x}$.

DOI: 10.1103/PhysRevB.104.075414

I. INTRODUCTION

The Klein paradox in single layer graphene (SLG), wherein electrons tunnel freely through a one-dimensional (1D) potential barrier, is due to the relativistic nature of graphene electrons [1–5]. If, in addition, the graphene sheet is subject to a perpendicular electric field, resulting in Rashba spin-orbit coupling (RSOC) [6], the role of the Klein paradox in graphene spintronics is revealed. Here we focus on the spin physics of electrons in SLG subject to a periodic 1D Kronig-Penney potential (1DKPP) $u(x)$, and uniform RSOC of strength λ. The main object of study is the equilibrium spin current density (ESCD), to be distinguished from transport spin current [7–13], that is a central observable in contemporary spintronics [14], and in particular, in graphene spintronics [15–17]. The physical meaning of $J_{ij}(\mathbf{r})$ is that electrons with spin s_i $(i = x, y, z)$ flow with velocity v_j $(j = x, y)$. The space dependence of $J_{ij}(\mathbf{r})$ is related to the occurrence of a spin torque density through the continuity equation [8]. A proposal for its measurement is detailed in Ref. [9]. The precise definition of equilibrium spin current is detailed elsewhere [10].

ESCD was calculated *in bulk SLG* subject to RSOC in Ref. [13] (where the Klein paradox and Bloch physics are absent) while in Ref. [18] the *transport spin current* for electron tunneling through a rectangular barrier is analyzed. In Ref. [19], the physics is focused on the Bloch spectrum and *transport spin polarization*. In the present study, the role of the Klein paradox is central. Because the 1DKPP depends only on x, the transverse wave number k_y is conserved. As shown in Refs. [1–5] the effect of the Klein paradox is most striking in the forward direction $k_y = 0$, wherein the transmission is unimpeded. In the presence of RSOC, the case $k_y = 0$ is rather peculiar: In the nonrelativistic formulation, the RSOC can be "gauged away" while for relativistic dynamics it cannot (see short discussion below). Hereafter we focus on the case $k_y = 0$.

Below, the spin current densities are calculated in terms of Bloch wave functions $\{\psi_p(x)\}$ [p is the crystal (Bloch) wave number], the spin density operator $\hat{\mathbf{S}}$, and the velocity operator $\hat{\mathbf{V}}$. Their properties are remarkably different from those predicted in bulk SLG [13], i.e., in the *absence* of a 1D potential wherein the Klein paradox does not play a role. The novel features exposed here are (1) While the local velocity vector $\mathbf{V}(x) = \psi_p^\dagger(x)\hat{\mathbf{V}}\psi_p(x)$, *and* the spin density vector $\mathbf{S}(x) = \psi_p^\dagger(x)\hat{\mathbf{S}}\psi_p(x)$ vanish (due to reflection symmetry [19]), yet, there are nondiagonal elements of the ESCD tensor $J_{ij} = \frac{1}{2}\psi_p^\dagger(x)\{\hat{V}_i, \hat{S}_j\}\psi_p(x)$ that are finite. Remarkably, unlike in bulk SLG [13], $J_{zy} \neq 0$. In other words, there is finite ESCD wherein electrons are polarized *perpendicular to the SLG plane*. (2) $J_{ij}(x)$ is space-dependent, hence there is a finite spin torque density [8]. (3) The response of the spin current densities to the RSOC strength λ is substantial even for small λ (the magnitude of λ due to a strong perpendicular electric field in SLG, as reported in Refs. [15,20], is a fraction of meV). These predictions are experimentally verifiable and are important for graphene spintronics.

The paper is organized as follows: Sec. II presents the formalism used. Section III specifies the parameters used in the calculations. Section IV presents the results, where Sec. IV A describes the Bloch spectrum, Sec. IV B gives the Bloch wave functions, and Sec. IV C discusses local observables. Finally, Sec. V presents a summary and a perspective.

II. FORMALISM

The basic ingredients for calculating ESCD are the Bloch spectrum and wave functions. Our method for obtaining the Bloch spectrum is similar to that used in Ref. [19]. It is briefly reformulated here because we need also the Bloch wave functions. Consider a system of massless 2D Dirac electrons in SLG lying on the x-y plane subject to a uniform electric field $\mathbf{E} = E_0\hat{\mathbf{z}}$ and a 1DKPP

$$u(x) = u_0 \sum_{m=-\infty}^{\infty} \Theta(x - m\ell)\Theta(m\ell + d - x), \tag{1}$$

of period $R = d + \ell$. As shown in Ref. [18], the Klein paradox (wherein electrons propagate under the barriers) occurs for $u_0 > \varepsilon + 2\lambda > 0$ where ε is the Fermi energy. To derive the Bloch spectrum, Bloch wave functions, and predict spin related observables, the problem is treated within the continuum formulation near one of the Dirac points, say $\mathbf{K}'$. Note that, in addition to the isospin $\boldsymbol{\tau}$ encoding the two-lattice structure of SLG, there is now a *real spin*, $\boldsymbol{\sigma}$. Wave functions and operators are then defined in the 4D $\boldsymbol{\sigma} \otimes \boldsymbol{\tau}$ (spin⊗isospin) space. We focus on the Bloch states $\{\psi_p(x)\}$ and Bloch energy $\varepsilon(p, \lambda)$ (in what follows, the (p, λ) dependence is occasionally dropped). We use units such that the kinetic energy parameter $\gamma \equiv \hbar v_F = 1$ ($v_F \approx 10^8$ cm/sec is the Fermi velocity). Consequently, lengths are given in nm, while wave numbers k_x, q_x, q_y [defined below in Eq. (5)], energies ε, u_0 and the RSOC strength λ are given in $(\text{nm})^{-1}$. In particular, $\lambda \propto 1/\ell_{so} \propto E_0$, where ℓ_{so} is the spin-orbit length [21]. However, in presenting our numerical results, energies ε, u_0 and λ are presented in meV.

The RSOC due to a uniform perpendicular electric field $\mathbf{E} = E_0\hat{\mathbf{z}}$ is introduced as an SU(2) vector potential $\mathbf{A} = \lambda\hat{\mathbf{z}} \times \boldsymbol{\sigma}$. Because k_y is conserved, the wave function is factored as $\Psi(x, y) = e^{ik_y y}\psi(x)$ [$\psi(x)$ is a four-component spinor in $\boldsymbol{\sigma} \otimes \boldsymbol{\tau}$ space].

Here we take $k_y = 0$, and a few words on the significance of this special case are in order. In the *nonrelativistic formulation* of RSOC for an electron in 2D (where only real spin is relevant, there is no isospin), the Schrödinger equation for *the two component spinor* $\phi(x)$ (with $2m/\hbar^2 = 1$ and for *any* k_y) reads,

$$[(-i\partial_x + \lambda\sigma_y)^2 + (k_y - \lambda\sigma_x)^2 + u(x)]\phi(x) = \varepsilon\phi(x). \tag{2}$$

But if (and only if) $k_y = 0$ the second term on the LHS of Eq. (2) is just λ^2 and then, the RSOC can be "gauged out". On the other hand, *in the relativistic formulation* that is relevant here, the system Hamiltonian (with $k_y = 0$) reads

$$h(-i\partial_x, \lambda) = [-i\partial_x + \lambda(\hat{\mathbf{z}} \times \boldsymbol{\sigma})_x]\tau_x + [\lambda(\hat{\mathbf{z}} \times \boldsymbol{\sigma})_y]\tau_y + u(x) \equiv h_0(-i\partial_x, \lambda) + u(x). \tag{3}$$

This Hamiltonian is a 4×4 matrix first-order differential operator. Because the Hamiltonian now contains *both* σ_x and σ_y, the RSOC *cannot* be "gauged out". Thus, the fact that RSOC is relevant even for $k_y = 0$ is a relativistic property.

The Hamiltonian in Eq. (3) acts on a Bloch function $\psi_p(x)$ that is a combination of four component plane wave vectors (the subscript p will occasionally be omitted),

$$\psi(x) = \sum_{n=1,s=\pm}^{2} \begin{cases} a_{ns}e^{isk_{xn}x}v_{ns}, & [u(x) = 0], \\ b_{ns}e^{isq_{xn}x}w_{ns}, & [u(x) = u_0]. \end{cases} \tag{4}$$

The squares of the wave numbers, depending on the (yet unknown) Bloch energy ε read [18],

$$k_{xn}^2 = [\varepsilon + (-1)^{n+1}\lambda]^2 - \lambda^2,$$
$$q_{xn}^2 = [\varepsilon + (-1)^{n+1}\lambda - u_0]^2 - \lambda^2. \tag{5}$$

The four components vectors $v_{ns}[sk_{xn}(\varepsilon)]$ and $w_{ns}[sq_{xn}(\varepsilon)]$ are straightforwardly computable (see Ref. [18] for explicit expressions). The constants $a_{ns}(\varepsilon)$ and $b_{ns}(\varepsilon)$ ($n = 1, 2$, $s = \pm$), are determined by matching the wave functions on the walls of the barrier and employing the Bloch condition.

Consider the unit cell $[0, R]$ consisting of the barrier region $[0, d]$ and the spacing between the barrier rgion $[d, d + \ell = R]$, corresponding to the $m = 0$ region in Eq. (1). Matching of the wave functions at the left wall of the barrier $x = 0$ requires $\psi(0^-) = \psi(0^+)$. It can be written in terms of $\{a_{ns}\}$, $\{b_{ns}\}$ using the following notation:

$$\mathbf{a} = (a_{1^+}, a_{2^+}, a_{1^-}, a_{2^-})^T,$$
$$\mathbf{b} = (b_{1^+}, b_{2^+}, b_{1^-}, b_{2^-})^T. \tag{6}$$

$\mathbf{a}$ and $\mathbf{b}$ are the 4×1 column vectors of coefficients introduced in Eq. (4). Moreover,

$$V = (v_{1^+}, v_{2^+}, v_{1^-}, v_{2^-}),$$
$$W = (w_{1^+}, w_{2^+}, w_{1^-}, w_{2^-}), \tag{7}$$

are 4×4 matrices built from the 4×1 column vectors introduced in Eq. (4). The matching equations at $x = 0$ and the transfer matrix carrying $\psi(0^-)$ to $\psi(0^+)$ are then given by

$$V\mathbf{a} = W\mathbf{b}, \ \Rightarrow \ T_{0^-\to 0^+} = W^{-1}V, \tag{8}$$

implying $T_{0^-\to 0^+}\,\mathbf{a} = \mathbf{b}$. Similarly, the transfer matrix carrying $\psi(d^-) \to \psi(d^+)$ across the right wall of the barrier is $T_{d^-\to d^+} = V^{-1}W$. To complete the construction of the transfer matrix $T_{0^-\to R^-}$ that carries the wave function across a unit cell from $[0, R]$, recall that the propagation of $\psi(x)$ from $0^+ \to d^-$ and from $d^+ \to R^-$ is, respectively, controlled by the 4×4 diagonal phase-factor matrices,

$$\Phi_q = \text{diag}[e^{iq_{x1}d}, e^{iq_{x2}d}, e^{-iq_{x1}d}, e^{-iq_{x2}d}],$$
$$\Phi_k = \text{diag}[e^{ik_{x1}\ell}, e^{ik_{x2}\ell}, e^{-ik_{x1}\ell}, e^{-ik_{x2}\ell}], \tag{9}$$

which leads to the expression

$$T \equiv T_{0^-\to R^-} = \Phi_k T_{d^-\to d^+}\Phi_q T_{0^-\to 0^+}. \tag{10}$$

T is a symplectic 4×4 matrix satisfying $\text{Det}[T] = 1$ and $T^\dagger\Sigma_z T = \Sigma_z$, where $\Sigma_z = \mathbf{1}_2 \otimes \tau_z$. The Bloch theorem for fixed λ, u_0, d and ℓ requires that $\psi(x + R) = e^{ipR}\psi(x)$. This implies the eigenvalue equation

$$T(\varepsilon)\mathbf{a}(\varepsilon) = e^{ipR}\mathbf{a}(\varepsilon). \tag{11}$$

Equation (11) defines a relation between the four eigenvalues $\{\lambda_j(\varepsilon)\}$ ($j = 1, 2, 3, 4$) of $T(\varepsilon)$ and the Bloch wave number p, i.e., $\text{Im}[\lambda_j(\varepsilon)] = \sin pR$. This gives the dispersion curves $\varepsilon_j(p) = [\text{Im}\lambda_j]^{-1}(\sin pR)$. The eigenvalues of $T(\varepsilon)$ satisfy the equalities $\lambda_1 = 1/\lambda_2$ and $\lambda_3 = 1/\lambda_4$, so that if $\lambda_j(\varepsilon)$ is

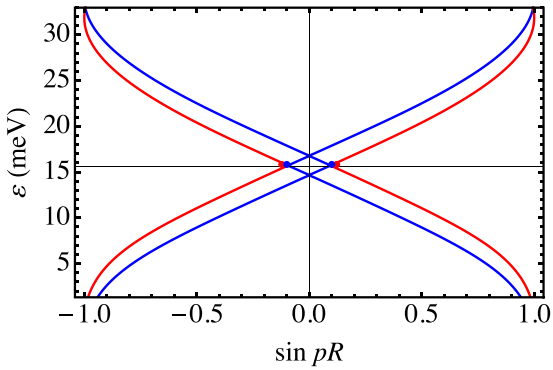

FIG. 1. Bloch spectrum for 1DKPP with $u_0 = 98.85$ meV, $d = 200$ nm, $\ell = 260$ nm and $\lambda = 1.0054$ meV. The figure shows the highest electron-hole energy curves $\varepsilon(p)$ for $k_y = 0$. In the absence of RSOC, all points coalesce into a single Dirac cone. Thus, RSOC causes level repulsion in both energy and Bloch wave number variables, leading to a rich pattern consisting of four Dirac points. The thin line at energy $\varepsilon = 15.873$ meV intersects the curves at four points (blue and red in the figure), $\varepsilon(p_i)$, $i = 1, 2, 3, 4$. The four wave functions $\{\psi_{p_i}(x)\}$ are used below to calculate the spin current densities.

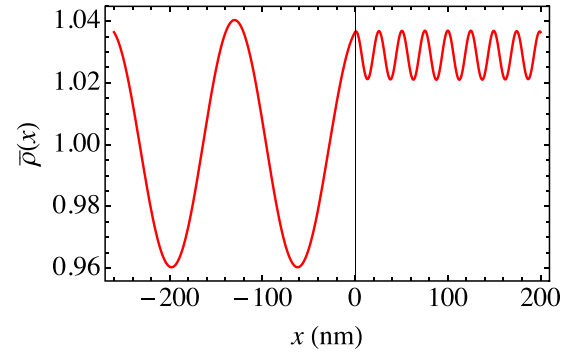

FIG. 2. Scaled density $\bar{\rho}(x)$ [defined after Eq. (12)] at Bloch energy $\varepsilon = 15.873$ meV] for $u_0 = 98.85$ meV, in a unit cell with $-l < x < d$ for $\lambda = 1.0054$ meV.

real, the energy $\varepsilon_j(p)$ is in the gap. Otherwise, the eigenvalues consist of two pairs of complex conjugate numbers lying on the unit circle, renumbered as $\lambda_1 = 1/\lambda_1^*$, $\lambda_2 = 1/\lambda_2^*$. Consequently, there are *two symmetric dispersion curves* $\varepsilon_1(p) = \varepsilon_1(-p)$ and $\varepsilon_2(p) = \varepsilon_2(-p)$ corresponding to the two SO split levels. For $\lambda \to 0$, the two curves coincide, forming valence and conduction bands that have a Dirac point at $p = 0$, with *linear dispersion*. As we shall see below, for $\lambda > 0$ there is level repulsion implying four Dirac points, but no gap is opened.

III. CHOICE OF PARAMETERS

It is important to choose potential parameters u_0, d, ℓ and RSOC strength λ in accordance with attainable values relevant for graphene. The magnitude of λ is dictated by experiments on Rashba spin-orbit splitting in SLG. In Ref. [15,20], it is shown that λ is in the order of fraction of 1 meV. In addition, the Bloch formulation implies that the wave numbers k_{xn} and q_{xn} should be real [see Eq. (5)]. This implies the inequality $\varepsilon > 2\lambda$ (for real k_{xn}) and $(u_0 - \varepsilon)^2 + 2\lambda(u_0 - \varepsilon) > 0$ for q_{xn}. Explicitly: The fixed parameters are: $u_0 = 98.85$ meV, $d = 200$ nm, $\ell = 260$ nm, hence $R = 460$ nm.

IV. RESULTS

A. Results–Bloch Spectrum

The Bloch spectrum $\varepsilon(p, k_y)$ (for any k_y), was calculated in Ref. [19] for $\lambda = 5$ meV, and intrinsic SO coupling of order 0.05 meV (see Fig. 6(a) therein). Following our discussion above concerning the experimental limits on the SO splitting, we choose λ to be less than 1.0054 meV. For fixed $k_y = 0$, the Bloch spectrum then displays four Dirac points as shown in Fig. 1. The dispersion at these four Dirac points remains linear, unlike in the pattern encountered in bulk SLG [15]. It is checked that in the absence of RSOC ($\lambda = 0$), the levels coalesce into a single Dirac point at $p = 0$ (with linear dispersion). Thus, RSOC results in level repulsion but keeps the gap closed (of course, in the absence of intrinsic SO coupling, small gaps are opened). From the point of view of band structure, the central rhombus in Fig. 1 can be viewed as a narrow "semimetallic band" between the wide valence and conduction bands.

B. Bloch wave functions

Calculations of the Bloch wave functions are carried out at a given Fermi energy $\varepsilon = 15.873$ meV, see the horizontal thin line in Fig. 1 that passes through the two Dirac points at $\sin pR = \pm 0.088$. The energy is fourfold degenerate, so there are *four wave functions*

$$\{\psi_{p_i}(x)\}, \text{ with } p_1 = -p_4,\ p_2 = -p_3,$$

corresponding to the four points $\{\varepsilon(p_i)\}$ marked on the thin line on Fig. 1 at which the constant energy line crosses the four dispersion curves. Explicit expressions of the wave functions are given in Eq. (4), wherein the coefficients $\{a_{ns}\}$ are the components of the vector **a** [defined in Eq. (6)] that is an eigenvector of the transfer matrix T with eigenvalue e^{ip_iR}. Similarly, the coefficients $\{b_{ns}\}$ are the components of the vector **b** defined after Eq. (8).

C. Local observables

Results–Local observables: An operator $\hat{O}$, is representable as a 4×4 Hermitian matrix in $\boldsymbol{\sigma} \otimes \boldsymbol{\tau}$ space. A *local observable* $O(x)$ related to the operator $\hat{O}$ takes the form

$$O(x) = \frac{1}{4}\sum_{i=1}^{4} \psi_{p_i}^{\dagger}(x)\hat{O}\psi_{p_i}(x), \tag{12}$$

(these are not expectation values). Below we consider operators of charge density, velocity, spin density and ESCD, and study the properties of the corresponding observables.

For the charge density, $\hat{O} = \mathbf{I}_4$. The (scaled) density $\bar{\rho}(x) \equiv \frac{1}{4}R\sum_{i=1}^{4} \psi_{p_i}^{\dagger}(x)\psi_{p_i}(x)$, is plotted as a function of position in Fig. 2 for $\lambda = 1.0054$ meV. It is characterized by oscillations around 1. The reason is that for $k_y = 0$, the Bloch waves propagate solely in the longitudinal direction and for $\lambda = 0$ the Klein paradox implies transmission coefficient for

tunneling through a barrier is unimpeded. Equivalently, for $\lambda = 0$ the Bloch functions are constant, $\psi_p(x) = 1/\sqrt{R}$. As shown in Ref. [18], for $\lambda > 0$, transmission slightly decreases. Consequently, the (scaled) density slightly deviates from its constant value and oscillates around 1. The higher frequency in the barrier region $0 < x < d$ (compared with those in the spacing region $-\ell < x < 0$) reflects the inequality of wave numbers [for the present choice of parameters $q_{xn} > k_{kn}$, see Eq. (5)].

Next we consider the velocity and spin density operators (the former is also the charge current operator),

$$\hat{\mathbf{V}} = \mathbf{I}_2 \otimes \boldsymbol{\tau}, \quad \hat{\mathbf{S}} = \tfrac{1}{2}\hbar\boldsymbol{\sigma} \otimes \mathbf{I}_2. \tag{13}$$

Employing Eq. (12), it is found that $\mathbf{V}(x) = 0$, (this is due to left-right antisymmetry, $V_x(x; p) = -V_x(x, -p)$ and to the fact that $k_y = 0$). Surprisingly, the velocity operator will contribute to the ESCD (see below). Of special relevance here is the fact that in relativistic quantum mechanics, e.g., in the Dirac equation where the Hamiltonian is $H_D = \boldsymbol{\alpha} \cdot \mathbf{p} + \beta m$, the velocity operator is $\boldsymbol{\alpha}$, and not $\mathbf{p}/m$ as in nonrelativistic quantum mechanics.

Inserting the spin density operators $\hat{\mathbf{S}}$ in Eq. (12) yields the observed spin density vector (polarization) $\mathbf{S}(x) = [S_x(x), S_y(x), S_z(x)]$. The units of the spin density is $S_0 = \hbar/A$. But in the present case, it is found that $\mathbf{S}(x) = 0$. The reason is that $\mathbf{S}(x) \parallel \mathbf{E} \times \mathbf{p}$ and for $k_y = 0$, $\mathbf{p} \parallel \hat{\mathbf{x}} \Rightarrow \mathbf{S}(x) \parallel \hat{\mathbf{y}}$ so that $S_x(x) = S_z(x) = 0$. In addition, contributions to $S_y(x)$ from $\pm p$ cancel.

The operator for the ESCD $\hat{\mathbb{J}}$ (a tensor) from which the components of the ESCD observables $J_{ij}(x)$ are derived via Eq. (12) are defined as

$$\hat{\mathbb{J}} = \tfrac{1}{2}\{\hat{\mathbf{S}}, \hat{\mathbf{V}}\}, \tag{14}$$

where $\hat{\mathbf{S}}$ and $\hat{\mathbf{V}}$ are defined in Eq. (13). The unit of ESCD J_{ij} is $J_0 = \frac{1}{2}\gamma/\text{nm}$: (spin density $= \frac{1}{2}\hbar/\text{nm}$)$\times$(velocity $= v_F$).

A beautiful manifestation of the combined effects of 2D Dirac electrons, Klein paradox, RSOC and Bloch theorem is that, although $\mathbf{V}(x) = 0$ and $\mathbf{S}(x) = 0$, nevertheless, $J_{xy}(x), J_{yx}(x), J_{zy}(x) \neq 0$. Indeed, see Eq. (12), and note that $\mathbf{V}(x; p)$ and $\mathbf{S}(x; p)$ are antisymmetric in p, hence $J_{ij}(x; p)$ is symmetric in p. These components of the spin density tensor are shown in Figs. 3(a), 3(b), and 3(c), respectively. They have oscillatory space dependence implying a nonzero torque (see below).

To determine the dependence of J_{ij} on λ we show in Fig. 3(d) the height of the middle peak of $J_{xy}(x)$ for $x < 0$ [see Fig. 3(a)] for $0 < \lambda < 1.3$ meV. The curve is well fit by the quadratic form, $\text{Max}(J_{ij}) = 0.939697\,\lambda + 0.446578\,\lambda^2$.

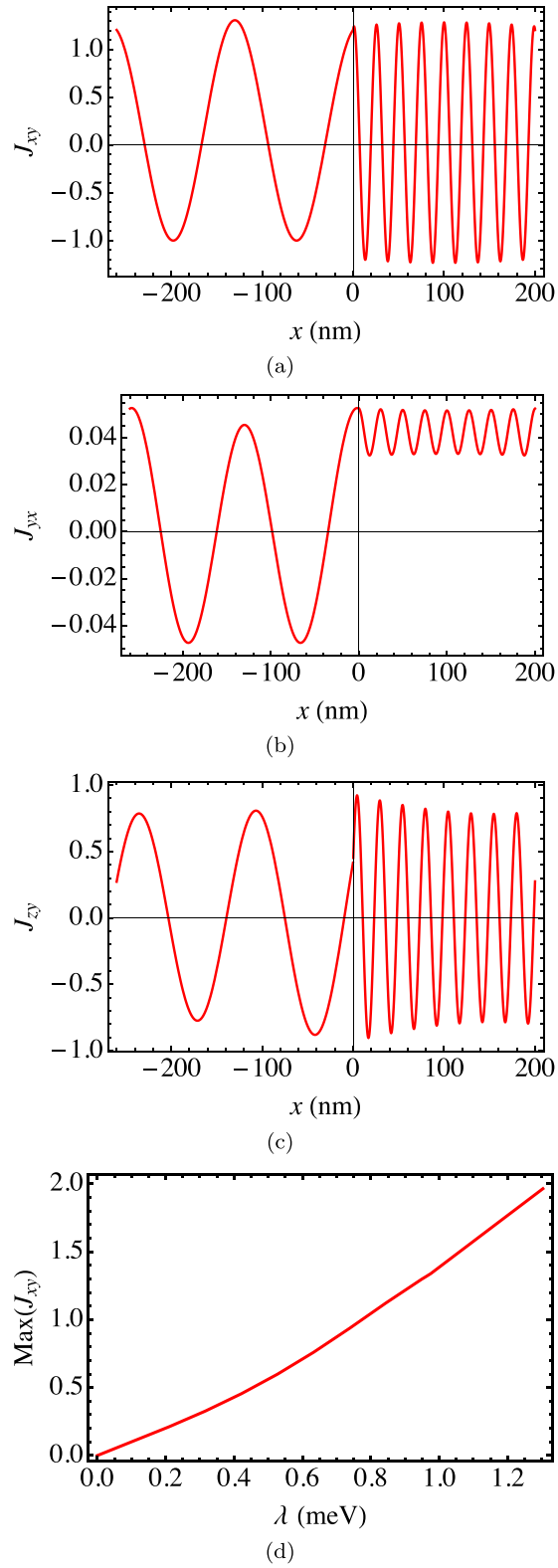

FIG. 3. Spin current densities in units of $J_0 = \frac{1}{2}\gamma/\text{nm}$] for $u_0 = 98.85$ meV, Bloch energy $\varepsilon = 15.873$ meV in the unit cell $-l < x < d$. (a) $J_{xy}(x)$, (b) $J_{yx}(x)$ and (c) $J_{zy}(x)$ for $\lambda = 1.0054$ meV. (d) Height of the central peak of $J_{xy}(x)$ as function of λ.

V. SUMMARY AND PERSPECTIVE

Let us compare our results for the ESCD with those in bulk SLG, as calculated in Ref. [13]. They found that (1) $J_{xx} = J_{yy} = J_{zx} = J_{zy} = 0$, (2) $J_{xy} = -J_{yx}$, (3) the spin currents is space-independent (see Eq. (5) in Ref. [13]), (4) The ESCD increases quadratically with λ [in their calculations λ was taken to be large; as high as $\lambda \approx 50$ meV]. (5) Higher Rashba splitting obtains if the SLG is in contact with metals such as Au and Pb, but then, in passing a current through such a slab, the electrons flow through the metal and not through the SLG, and, at the Fermi level, the electronic states are metallic.

In the presence of a 1DKPP (where there is no rotational symmetry around the z axis) the results are evidently different. We find that: (1) $|J_{xy}(x)| \neq |J_{yx}(x)|$. (2) Although the value of λ used in our calculations is about 1.5 orders of magnitude smaller than that used in Ref. [13], the size of the spin current densities in both systems are of the same order of magnitude. Moreover, the spin current does not increase quadratically as in bulk SLG. For small λ, it is dominated by a linear term. (3) $J_{zy}(x) \neq 0$ and the current is polarized perpendicularly to the plane (bear in mind the the system is invariant under time reversal). (4) The spin current densities are space dependent and, generically, the divergence of the ESCD does not vanish. Hence, the continuity equation contains a spin torque density term [8]. Specifically, the continuity equation for the vector field $\mathbf{J}_y(x) = [J_{yx}(x), 0]$ contains the spin torque density $\mathcal{T}_y(x) = dJ_{yx}(x)/dx$.

The role of the Klein paradox in graphene spintronics for systems invariant under time reversal has been mainly studied in the framework of scattering theory (tunneling through a barrier). In the present work, rather than focusing on barrier tunneling, we explore graphene spintronics through the properties of Bloch eigenstates by combining the following four pillars of graphene spintronics: 2D massless Dirac electrons, the Klein paradox, the Bloch theorem, and RSOC.

It is worth pointing out that in the problem of scattering through n-RSOC-n junction, the object of study is transport spin current, and it can be expressed in terms of the *spin resolved conductance* $G_{\sigma'\sigma}$ (see, *e.g.*, Refs. [22–24]). But here we focused on ESCD as defined in Refs. [8,9]. The two definitions are mutually exclusive because they refer to different physical situations.

Because the calculated spin current densities studied here are shown to have very different properties than those found in bulk SLG [13], it is our hope that within the experimental limit on the RSOC strength, the size of the ESCD reported here should be experimentally measurable. A suggestion for measuring spin current as considered here was presented in Ref. [7–10]. ESCD and transport spin current are distinct as they refer to different physical situations.

ACKNOWLEDGMENT

Discussions with J. Nitta, J. Fabian, K. Richter M. H. Liu, and E. B. Sonin are highly appreciated.

[1] M. I. Katsnelson, K. S. Novoselov, and A. K. Geim, Nat. Phys. **2**, 620 (2006).
[2] V. V. Cheianov and V. I. Falko, Phys. Rev. B **74**, 041403(R) (2006).
[3] C. W. J. Beenakker, Rev. Mod. Phys. **80**, 1337 (2008).
[4] T. Tudorovskiy, K. J. A. Reijnders, and M. I. Katsnelson, Phys. Scr. **T146**, 014010 (2012).
[5] P. E. Allain and J.-N. Fuchs, Eur. Phys. J. B **83**, 301 (2011).
[6] E. I. Rashba, Sov. Phys. Solid State **2**, 1109 (1960); Y. A. Bychkov and E. I. Rashba, JETP Lett. **39**, 78 (1984).
[7] Q. F. Sun and X. C. Xie, Phys. Rev. B **72**, 245305 (2005); Q. F. Sun, X. C. Xie, and J. Wang, Phys. Rev. Lett. **98**, 196801 (2008); Q. F. Sun, Phys. Rev. B **77**, 035327 (2008).
[8] J. Shi, P. Zhang, D. Xiao, and Q. Niu, Phys. Rev. Lett. **96**, 076604 (2006).
[9] E. B. Sonin, Phys. Rev. Lett. **99**, 266602 (2007).
[10] E. B. Sonin, Adv. Phys. **59**, 181 (2010).
[11] H.-J. Drouhin, G. Fishman, and J.-E. Wegrowe, Phys. Rev. B **83**, 113307 (2011).
[12] Z. An, F. Q. Liu, Y. Lin, and C. Liu, Sci. Rep. **2**, 388 (2012).
[13] H. Zhang, Z. Ma, and J. F. Liu, Sci. Rep. **4**, 6464 (2015).
[14] I. Zutic, J. Fabian, and S. Das Sarma, Rev. Mod. Phys. **76**, 323 (2004).
[15] W. Han, R. K. Kawakami, M. Gmitra, and J. Fabian, Nat. Nanotechnol. **9**, 794 (2014).
[16] L. Brey, Phys. Rev. B **92**, 235444 (2015); L. Chico, A. Latgé, and L. Brey, Chem. Phys. **17**, 16469 (2015).
[17] A. Avsar, H. Ochoa, F. Guinea, B. Özlimaz, B. J. van Wees, and I. J. Vera-Marun, Rev. Mod. Phys. **92**, 021003 (2020).
[18] Y. Avishai and Y. B. Band, Phys. Rev. B **103**, 134445 (2021).
[19] K. Shakouri, M. R. Masir, A. Jellal, E. B. Choubabi, and F. M. Peeters, Phys. Rev. B **88**, 115408 (2013).
[20] M. Gmitra and J. Fabian, Phys. Rev. B **92**, 155403 (2015).
[21] A. Shnirman, *Geometric Phases and Spin-Orbit Effects*, Lecture 2, Karlsruhe Institute of Technology. http://www.thp.uni-due.de/~koenig/DPG_School_10/Shnirman_2.pdf.
[22] M-H. Liu, J. Bundesmann, and K. Richter, Phys. Rev. B **85**, 085406 (2012).
[23] Y. Avishai and Y. B. Band, Phys. Rev. B **95**, 104429 (2017).
[24] H. Santos, A. Latgé, L. Brey, and L. Chico, Carbon **168**, 1 (2020).